Acta Cryst. (1988). A44, 810-820

Two-Beam Features in Electron Diffraction Patterns – Application to Refinement of Low-Order Structure Factors in GaAs

BY KJERSTI GJØNNES AND JON GJØNNES

Department of Physics, University of Oslo, Oslo, Norway

AND J. ZUO AND J. C. H. SPENCE

Department of Physics, Arizona State University, Tempe, Arizona, USA

(*Received* 23 *November* 1987; *accepted* 8 *April* 1988)

Abstract

Progress in theoretical approaches to the refinement of structure factors and structure determination by electron diffraction is briefly reviewed. A strategy based on the use of two-beam-like features in convergent-beam electron diffraction (CBED) patterns is advocated, based on an effective potential and a reduced excitation error. Model calculations suggest inversion of the Bethe potentials to be useful. New experimental measurements for CBED rocking curves in GaAs are reported and these give the refined values $V(200) = 0{\cdot}432$ (9), $V(400) = 4{\cdot}53$ (4) V at 90 K, including Debye-Waller factor. The results from the inverse Bethe potential method are in excellent agreement with full many-beam calculations. These experimental values are compared with the results of recent pseudopotential total-energy calculations.

1. Introduction

It is now almost forty years since the first attempts at crystal structure refinement by electron diffraction (Cowley, 1953; Vainshtein & Pinsker, 1950; MacGillavry, 1940). The early researchers were quick to realize certain advantages offered by electron scattering, *e.g.* the high sensitivity of low-order electron structure factor to charge transfer effects in crystals [for a discussion of the effects of ionicity and bonding on electron diffraction intensities, see Cowley (1953)]. The intervening period has seen vast advances in instrumentation, including the development of brighter electron sources, probe-forming optics for convergent-beam diffraction (CBED) and improved vacuum conditons for reduced contamination. The use of the new parallel detector systems with large (2^{12}) dynamic range, based on single-crystal screens bonded to cooled charge-coupled devices (Spence & Zuo, 1988), offers promise for greatly improved quantitative data collection. The developments in instrumentation have been exploited in different measurement techniques relating to structure factor measurement, *e.g.* the use of CBED fringes (Shishido & Tanaka, 1976; Goodman, 1976; Voss, Lehmpfuhl & Smith, 1980), the intersecting Kikuchi line (IKL) method (Taftø & Gjønnes, 1985), higher-order Laue zone (HOLZ) intensities (Vincent, Bird & Steeds, 1984) and critical-voltage CBED methods (Moodie, Humphreys, Imeson & Sellar 1978).

On the theoretical side progress appears to have been slower, despite the fact that the theory of dynamical Bragg diffraction of kilovolt electrons by a known crystal structure has been well understood for many years. The remaining problems seem to be connected more with the practical application of the theory to the determination of unknown structures than with further refinement of basic theory. This still presents a formidable task. Despite much effort using various types of diffraction patterns and despite the success in the accurate determination of a few structure factors for very simple structures, we still lack reliable procedures for structure determination by electrons to acceptable accuracy. There is as yet no obvious way to extract from the complete scattering pattern a set of well defined measurable quantities which can be introduced into a standard procedure for structure determination comparable to the use of integrated intensities in X-ray or neutron crystallography.

The aim is therefore to search for such quantities, which should be obtained from the CBED pattern and be related to structure factors. The use of the CBED method is essential. Experimental intensity in the form of two-dimensional rocking curves $I_g(k_x, k_y)$ is sampled from an area small enough to assume the crystal to be perfect and the orientation and thickness to be constant within the scattering volume. Hence the CBED intensities may be compared directly with theoretical calculations, in contrast with the intensity of the reflections in the small-angle diffraction (SAD) pattern. Typical CBED patterns (Figs. 1 and 6) are seen to contain a vast amount of details, which depend upon thickness, lattice constants and wavelength as well as several structure parameters in a complicated way. However, inspection of such patterns and of

0108-7673/88/060810-11$03.00

theoretical calculations reveal that much of the detail within the CBED disks (and in the Kikuchi pattern) has qualitative appearance similar to the two-beam case, even when many interacting beams are evident in the pattern. This applies particularly to the intensity profiles normal to the Kikuchi or Kossel lines. These profiles may tentatively be represented by the well known two-beam intensity expression

$$I_g(k_x, k_y) = \{U_g^2/[(ks_g)^2 + U_g^2]\} \times \sin^2\{(\pi z/k)[(ks_g)^2 + U_g^2]^{1/2}\} \quad (1)$$

if an 'effective Fourier potential', U_g^{eff}, is substituted for U_g. The maximum may be shifted from the Bragg position $s_g = 0$; in this case a reduced excitation error $s_g' = s_g - s_g^0$ should be substituted for s_g. These magnitudes, U^{eff} and s_g^0, will usually vary along the Kikuchi or Kossel line segments to which they relate, reflecting varying effects of simultaneously excited reflections.

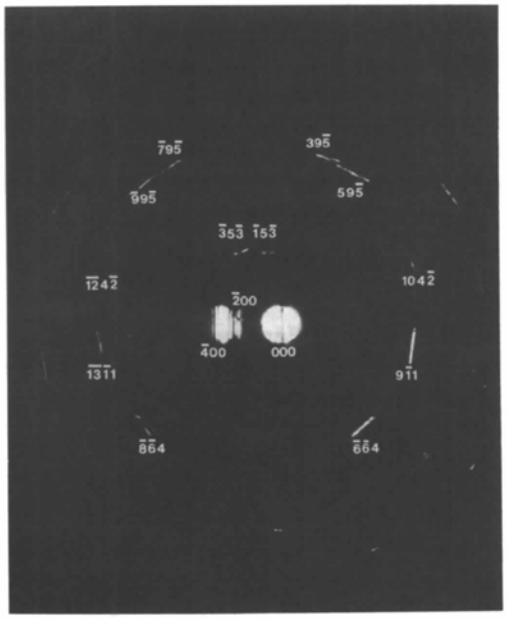

(*a*)

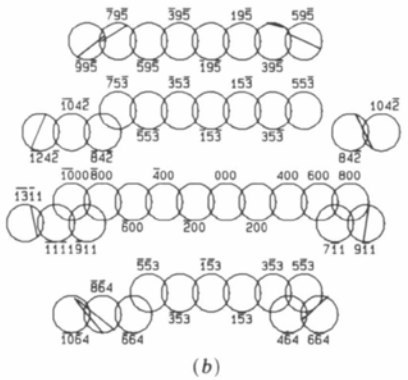

(*b*)

Fig. 1. (*a*) Experimental convergent-beam pattern recorded at 120 kV from GaAs at 90 K near the [035] zone axis showing the [*h*00] systematic row and accidental reflections. (*b*) Schematic diagram indicating the reflections included in the refinement of structure factors.

It is suggested in this paper that many intensity features in CBED patterns can indeed be represented by such an expression, that the parameters U^{eff} (and s_g^0) should be related to Bloch-wave pairs (i, j), that they can be extracted by different kinds of measurements, relating to positions of lines, to fringe patterns or to an integrated intensity, and that they can be related to structure factors by relatively simple expressions.

Our aim is to test the validity of such expressions for the effective potential (or its equivalent, the gap at the dispersion surface). Numerical calculations are presented for systematic rows in GaAs. Experimental intensity profiles for reflections along the [*h*00] row of GaAs are analysed and the structure factors for 400 and 200 are refined.

2. General theory and approximations

We commence with the familiar Bloch-wave solution for the Schrödinger equation (Reimer, 1984),

$$[K^2 - (\mathbf{k}+\mathbf{g})^2]C_g + \sum_h U_{g-h}C_h = 0, \quad (2)$$

where $K^2 = k_0^2 + U_0 = 2mE/h^2 + 2meV_0/h^2$, with E the accelerating voltage and U_g the Fourier coefficients of the crystal potential. For an incident electron beam near the surface normal this equation simplifies to

$$2k(s_g - \gamma)C_g + \sum_{h \neq g} U_{g-h}C_h = 0, \quad (2a)$$

where $\sum_g C_g \exp[2\pi i(\mathbf{k}+\mathbf{g})\mathbf{r}]$ are the Bloch waves with corresponding eigenvalues γ, and where the excitation error s_g is measured along the surface normal.

In the general case, *i.e.* with HOLZ reflections included (as in the refinement of experimental intensities presented below) or with an inclined surface, the 'zero-layer' form (2*a*) may be retained through a renormalization (Niehrs & Wagner, 1955; Gjønnes & Gjønnes, 1985). Let

$$\mathbf{k} = \mathbf{k}_0 + \gamma\mathbf{n}$$

where **n** is a unit vector along the surface normal. Using this equation in (2) and redefining the Bloch-wave coefficients

$$B_g = (1+g_n/K_n)^{1/2} C_g$$

we obtain

$$\frac{-B_g(2\mathbf{k}.\mathbf{g}+g^2)}{1+g_n/K_n} + \sum_{h\neq g} \frac{B_h U_{g-h}}{(1+g_n/K_n)^{1/2}(1+h_n/K_n)^{1/2}} = 2K_n\gamma B_g. \quad (3)$$

Here $g_n = \mathbf{g}.\mathbf{n}$ and $K_n = \mathbf{K}.\mathbf{n}$. Equation (3) has been solved numerically to obtain the refined values of GaAs structure factors which include HOLZ effects. Absorption may be included through an additional imaginary (non-Hermitian) potential, usually introduced as a perturbation, *i.e.* by an imaginary addition to the eigenvalues, γ.

Numerical solution of the eigenvalue equation (3) may work well in a final refinement or when the structure is known apart from one or two parameters. But for application to more general cases, it is desirable to have procedures for approximate solutions in terms of effective Fourier potentials or structure factors. We are then especially interested in features where two Bloch waves, i and j, dominate the expression for CBED contrast:

$$I_g(k_x, k_y) = \sum_i \sum_j C_0^i (C_g^i)^* (C_0^j)^* C_g^j \times \exp[-2\pi(\gamma^i - \gamma^j)z]. \quad (4)$$

In many such cases one structure factor (U_g) will be the main contribution to the gap, $(\gamma^i - \gamma^j)$, but this is not essential for the further discussion. Let us here outline briefly three ways of including the multiple-beam effects on 'two-Bloch-wave features': (i) beam reduction in symmetrical cases; (ii) perturbation expression for scattering between Bloch waves; (iii) the Bethe potentials.

In beam reduction the symmetry relations between Bloch-wave amplitudes at special points in the Brillouin zone are exploited. Several cases were treated by Fukuhara (1966). A general discussion of the planar point symmetry in symmorphic groups has been given by Taftø (1982). The dispersion surface and thickness-averaged intensity I_g are shown for two useful cases in Fig. 2.

Perturbation expressions for scattering between Bloch waves (interband scattering) have been applied to various problems in electron diffraction, *e.g.* to inelastic and other forms of diffuse scattering by Howie (1963), Gjønnes (1966) and others. Buxton (1976) treated HOLZ line intensities by essentially similar expressions. We shall here consider briefly scattering between two dense rows in a projection. In the usual forward scattering approximation this can be pictured as a sequence of scattering processes taking place at different levels in the object. The incident wave is scattered along the first row, *i.e.* into the beams $\mathbf{k}_0 + n\mathbf{h}$. At a level z these waves are scattered through the potentials U_{g+mh} into the other row, *i.e.* the beams $\mathbf{k}_0 + \mathbf{g} + n\mathbf{h}$, along which further scattering takes place. The amplitude for the beam g in the second row can now be written as

$$A_g(z) = \int_0^z \sum_h \sum_{g'} S_{gg'}(z-z') U_{g'h} S_{h0}(z')\, dz' \quad (5)$$

where the integration can be performed by expanding the scattering matrices, S, in Bloch waves, *viz*

$$A_g(z) = \sum_h \sum_{g'} \sum_i \sum_j (C_g^i)^* C_{g'}^i U_{g'h} C_h^j (C_0^j)^* \times \frac{\exp(i\gamma^i z) - \exp(i\gamma^j z)}{i(\gamma^i - \gamma^j)} \quad (5a)$$

where the (i,j) term may be seen as a 'quasikinematical' expression for scattering between the Bloch waves i and j, with maximum appearing when $\gamma^i = \gamma^j$, *i.e.* for a particular diffraction condition which can be measured - as in the IKL method. The strength of the interaction is given by the matrix element $\langle i|U|j\rangle = U^{\text{eff}}$. The z-dependent term

$$\frac{\exp(i\gamma^i z) - \exp(i\gamma^j z)}{i(\gamma^i - \gamma^j)}$$

is a function of the difference $(\gamma^i - \gamma^j)$ only, *i.e.* the distance between the two branches. In the kinematic approximation this depends on an excitation error, s. In the two-beam case

$$\gamma^i - \gamma^j = [s^2 + (U/k)^2]^{1/2} \quad \text{and} \quad \gamma^i + \gamma^j = s.$$

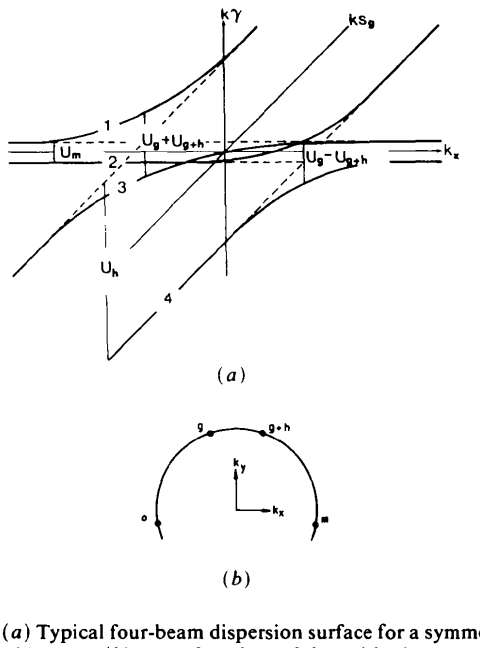

Fig. 2. (*a*) Typical four-beam dispersion surface for a symmetrical separable case (*b*) as a function of k_y, with the gap values indicated.

An approximation beyond the kinematic form in (5*a*) is obtained by substituting the equivalent two-beam-like expression based on U^{eff} for the z-dependent term in (5*a*), *i.e.*

$$\frac{U^{\text{eff}}}{[(U^{\text{eff}}/2k)^2+(s/2)^2]^{1/2}} \times \sin\{[(U^{\text{eff}}/2k)^2+(s/2)^2]^{1/2}z\}\exp(is/2)$$

is substituted for

$$U_{g'h}\frac{\exp(i\gamma^i z)-\exp(i\gamma^j z)}{i(\gamma^i-\gamma^j)}$$

in (5*a*). In this way we may also define an integrated intensity similar to the Blackman (1939) formula for the pure two-beam case.

The Bethe (1928) potential is a perturbation approach directly on the eigenvalue. This was introduced in order to include the effect of weak beams on the two strong beams in the form

$$U_g^{\text{eff}} = U_g - \sum_{h\neq g} U_h U_{g-h}/2ks_g. \qquad (6)$$

Despite certain limitations at small thicknesses (Gjønnes, 1962) this approximation works well in many cases. It is very useful in the treatment of the systematic row, which we now consider in more detail, first through model calculations.

3. Calculations for the systematic row

Numerical calculations were performed for systematic rows in several substances, with two main objectives, *viz* to test the representation of intensity profiles as a function of the diffraction condition s_g by two-beam-like expressions and to test approximations for U^{eff}. The dynamical n-beam calculations were performed for a wide range of incident-beam directions. The results reported here are for [*h*00] and [*hhh*] rows in GaAs. A sufficient number, typically about 20, of symmetrically placed beams in the systematic row were used. The results are presented in Figs. 3 to 5 as dispersion surfaces, rocking curves at selected thicknesses and as thickness averages for the different reflections. The two-Bloch-wave character is illustrated by the magnitude $|C_0^j|^2+|C_0^i|^2$. The calculations were performed without absorption, since they were aimed at the form of the solution and its representation by the gap, U^{eff}, as parameter.

We have drawn the dispersion surface (Figs. 3, 4 and 5) with k_x as the abscissa, *i.e.* Bloch-wave eigenvalues and excitation errors are shown as functions of the x component of the wave vector **k** for the incident electrons. The motivation for this representation (rather than the one found in most text books) is that the x and y components of **k** are also the coordinates within the CBED disks, and can thus be measured directly in the diffraction pattern. Dispersion surfaces in Figs. 3, 4 and 5 thus give the variation of γ^j and s_g as traced across the CBED disks (perpendicular to the K lines) for different orientations.

The dispersion surface is a useful indication of the two-Bloch-wave character. The [*h*00] row in GaAs (Fig. 3*a*) is a good example. The gaps are well separated, with a hyperbolic shape of the two branches around the Brillouin zone boundaries. For the [*hhh*] row (Fig. 3*b*) there is more overlap between neighbouring gaps, and here the two-Bloch-wave description is clearly poorer. This is reflected in the magnitude $|C_0^j|^2+|C_0^i|^2$, *i.e.* the fraction of the total intensity included in the two branches forming the gap. Figs. 3(*c*) and (*d*) show this for the different gaps along the two rows [*h*00] and [*hhh*].

A more detailed test of the two-Bloch-wave representation is provided by the comparisons in Fig. 4.

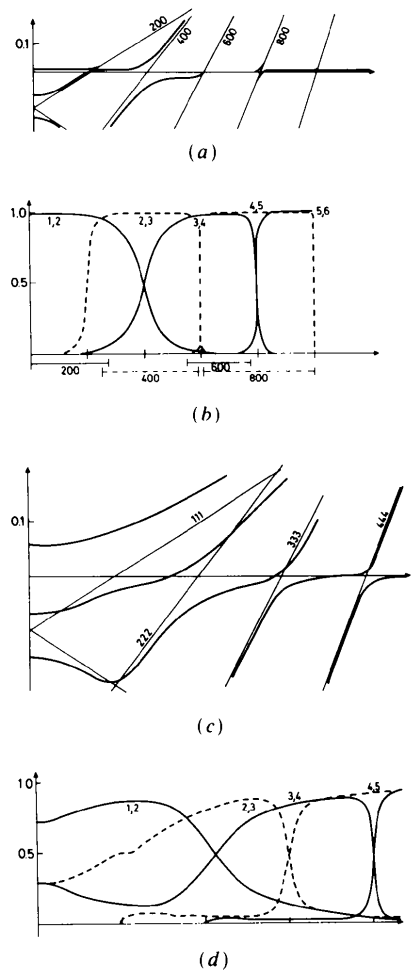

Fig. 3. Bloch-wave calculations for the [*h*00] and [*hhh*] systematic rows in GaAs at 120 kV. (*a*) Calculated dispersion surface for the [*h*00] systematic row. (*b*) Intensity in Bloch-wave pairs in the [*h*00] row. (*c*) Calculated dispersion surface for the [*hhh*] systematic row. (*d*) Intensity in Bloch-wave pairs in the [*hhh*] row.

Here the shape of the two branches forming the gap and their separation $k(\gamma^i - \gamma^j)$ as a function of the beam direction, given by k_x, are compared with the two-beam expressions using either the structure factors U_g or the calculated gap U_g^{eff} as parameter. Included in these figures are also the thickness-averaged rocking curves.

In a further set of curves (Fig. 5) exact calculations of [h00] rocking curves at two thicknesses, 100 and 200 nm, are compared with standard two-beam calculations and with two-beam expressions using the exact value for the gap. The comparisons show that the introduction of the gap as an effective potential always leads to a marked improvement over the two-beam-type expression. The two-Bloch-wave character varies: the reflections along the [h00] row are much better represented by two Bloch waves than those along the more dense [hhh] row; note the very good fit for 400 and 800.

The value of the gap at the dispersion surface, $k(\gamma^i - \gamma^j)$, or U^{eff}, may differ considerably from the two-beam value. Several approximations may be used to calculate U^{eff}. The Bethe formula was found to give a good fit in the [h00] row (see Table 1). For

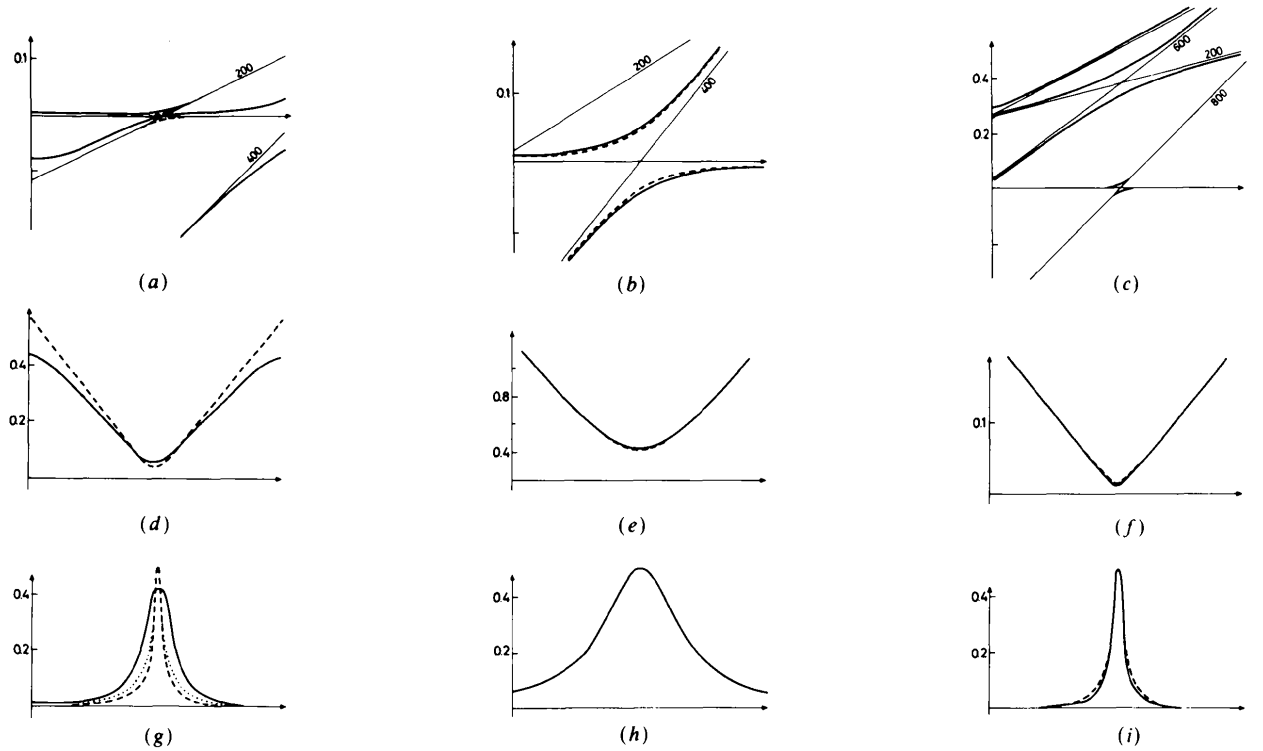

Fig. 4. Comparison between full n-beam calculations (solid curve), two-beam calculations (dashed curves) and two-Bloch-wave calculations (dotted curves) for the [h00] systematic row in GaAs at 120 kV. (a), (b) and (c) Dispersion surface near the Bragg condition for 200, 400 and 800 respectively. (d), (e) and (f) Distance between the two branches at the dispersion surface near the gap at the Bragg condition for 200, 400 and 800. (g), (h) and (i) Thickness-averaged rocking curves for 200, 400 and 800.

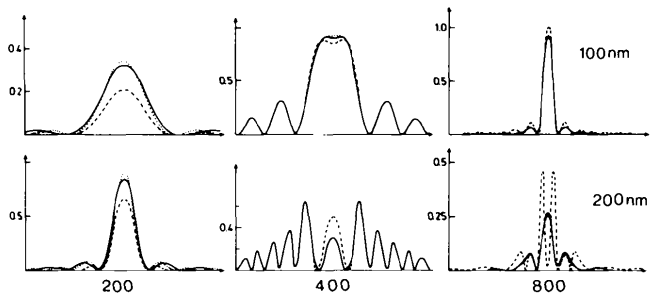

Fig. 5. Intensity profiles in the [h00] row in GaAs at 120 kV at 100 and 200 nm. Comparison between full n-beam calculations (solid curve), two-beam calculations (dashed curves) and two-Bloch-wave calculations (dotted curves).

Table 1. *Structure factors, gaps at the dispersion surface and approximations for* GaAs, *with the systematic row* [*h*00] *at* 120 kV (*structure factors and gaps are given in* Å^{-2})

h k l	U_g	$k(\gamma^i-\gamma^j)$	U_g^{Bethe}	U_g^*
2 0 0	0·00450	0·00595	0·00600	0·00483
4 0 0	0·04104	0·04205	0·04221	0·04131
6 0 0	0·00031	0·00084	0·00087	0·00042
8 0 0	0·01548	0·01237	0·01251	0·01539
10 0 0	0·00023	0·00005	0·00000	0·00030
12 0 0	0·00640	0·00530	0·00526	0·00645
14 0 0	0·00013	0·00008	0·00006	0·00015
16 0 0	0·00269	0·00228	0·00226	0·00271
20 0 0	0·00114	0·00097	0·00098	0·00113
24 0 0	0·00047	0·00041	0·00046	0·00048

U_g is the structure factor calculated from the known structure of GaAs and Doyle–Turner scattering factors for electrons.

$k(\gamma^i-\gamma^j)_{\min}$ is the corresponding gap at the dispersion surface, *i.e.* the minimum distance between Bloch waves i and j near $s_g=0$.

$U_g^{\text{Bethe}}=U_g-\sum_{h\neq g}U_hU_{g-h}/2ks_h$ is the Bethe potential.

U_g^* is the approximation to U_g derived from the inverse Bethe formula (see Appendix).

the [*hhh*] row the Bethe approximation gave a much poorer fit - as was expected from the dispersion surface.

The good fit to exact calculations using the Bethe formula suggested that a reverse procedure be tried: we may obtain the Fourier potentials from the gaps by taking, for example, the largest gap as a starting value and correcting the gaps through an iteration procedure. As a first step a computer program for deriving the potentials from the gaps was written and applied to the values for the gaps previously obtained from the many-beam calculations listed in Table 1. This procedure, which is outlined in the Appendix, was found to converge and produced the values listed in the last column of Table 1. The procedure was tried in a number of cases, and was found to work well when there is a marked two-Bloch-wave character.

The next step in these computational exercises was to try methods to extract the gap values from intensity profiles. The method must be adapted to gaps of different sizes: For large gaps, when there is a well developed fringe pattern, procedures similar to those used by Goodman & Lehmpfuhl (1967) and in later studies can be used, *i.e.* determination of thickness from the outer part of the fringe pattern followed by curve fitting in the central part in order to determine the gap. For small gaps an integrated intensity of the profile across the Kossel line must be determined and normalized to the profile of a larger gap. For thicknesses small relative to the gap this integrated intensity will be proportional to the square of the gap, *i.e.* to $(U^{\text{eff}})^2$. At greater thickness this kinematical integral should be replaced by the expression introduced by Blackman (1939) for the integrated intensity across a two-beam profile [see equation (*A*9)].

Table 2. *Test of the application of the two-beam description to determination of structure factors*

Determination of approximations to U_{200}, U_{400} and U_{800}, and the corresponding gaps, in GaAs from simulated intensity profiles (*n*-beam calculations) (structure factors and gaps measured in Å^{-2}).

g	Structure factors	Gap at the dispersion surface (from *n*-beam calculation)	Approximation to the gap at the dispersion surface	Approximation to U_g derived from the inverse Bethe formula and the approximate gaps
2 0 0	0·00507	0·00689	0·00615*	0·00447
4 0 0	0·04625	0·04748	0·04746†	0·04601
8 0 0	0·01745	0·01347	0·01314‡	0·01760

* From the ratio between the integrated intensity in 200 and 400.

† From least-squares fit of the intensity profile to a two-beam expression with the thickness and the effective structure factor as parameters.

‡ As † but with known thickness.

Such a procedure was tried on the [*h*00] row. Starting from the computed intensity profiles at a given thickness (200 nm), the calculations were run backwards: from the 400 profile the thickness and gap were obtained, and similarly for the 800, whereas the 200 gap was derived from the integrated intensity. These values were then introduced in the iteration scheme based on the Bethe potential formula. Results are summarized in Table 2.

4. Experimental

Experimental measurements were made of the 200 and 400 rocking curves in CBED patterns from thin (110) samples of GaAs prepared by mechanical dimpling and ion milling. By comparing these experimental CBED intensity profiles with many-beam Bloch-wave computations, values of the structure factors have been refined. Through application of the procedures explained in the previous section, the accuracy and utility of the Bethe series inversion and the two-beam form could also be tested on experimental curves.

Energy filtered intensity data were collected in a Philips EM 400T electron microscope through an energy loss spectrometer (Gatan, model 607) using a deflection system under computer (PDP11/23) control to scan the pattern over a 1 mm slit. Fig. 6 compares the measured energy-filtered intensity across 000, 200 and 400 with the observed diffraction pattern. For a camera length of 460 cm this corresponds to an angular resolution of 1·8% of the 002 diffraction angle. An electron probe size of 400 nm was used at the accelerating voltage 120 ± 0·5 kV as determined by the Kikuchi line/HOLZ method (Fitzgerald & Johnson, 1984). The range of thickness under the probe was confirmed to be very small by observation of *Pendellösung* fringes. The orientation near [035] (see Fig. 1) was chosen so as to minimize the excitation of reflections other than the *h*00 systematics; however, our calculations were not restricted to these.

The choice of camera length, detection aperture, spot size (source intensity), number of scan points (150), dwell time (0·8 s) and probe size were determined by the required compromise between sample stability, uniformity of thickness, electron emission stability and the required signal-to-noise ratio. The sample was cooled to 90 K in order to minimize phonon scattering and reduce contamination.

The adjustable parameters in our refinement included crystal thickness, the 200 and 400 structure factors, the specimen orientation (*i.e.* the effect of non-systematic and HOLZ reflections), accelerating voltage and the absorption coefficients. The general refinement strategy was as follows: (i) The accelerating voltage and orientation were determined from the position of HOLZ lines crossing the central disk and the outer HOLZ reflections. (ii) The absorption coefficients were determined by matching the asymmetry of the 000 rocking curve. (iii) The specimen thickness was determined by matching the outer fringes in the CBED disks accurately. (iv) The structure factors of 200 and 400 were then derived essentially from the central portion of the CBED disk (near the Bragg condition); in particular the relative heights of

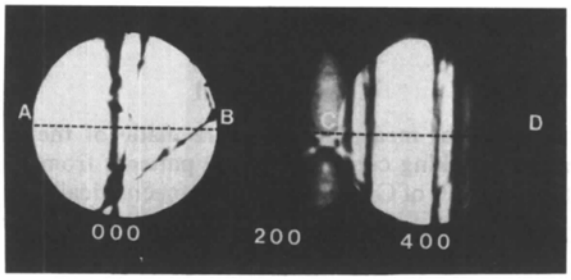

(*a*)

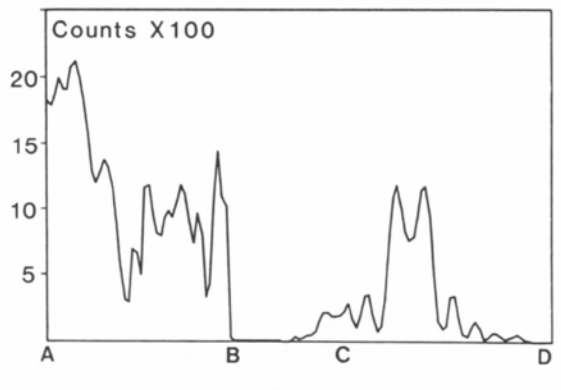

(*b*)

Fig. 6. (*a*) CBED pattern from GaAs recorded at 120 kV and 92 K showing the line along which the energy-filtered intensity measurements in (*b*) were taken. (*b*) Experimental energy-filtered elastic scattering intensity along the line shown in (*a*). Abscissa calibration: at *A*, $(k_x, k_y, k_z) = (2{\cdot}75, -1{\cdot}175, 0{\cdot}705)$ and at *B*, $(k_x, k_y, k_z) = (0{\cdot}55, -1{\cdot}175, 0{\cdot}705)$ in fractional reciprocal-lattice units.

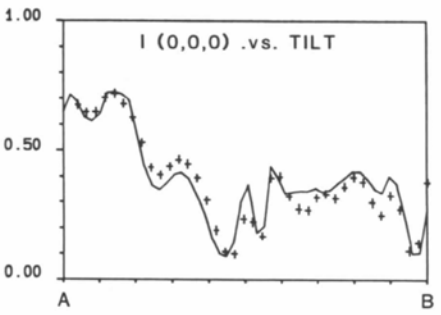

(*a*)

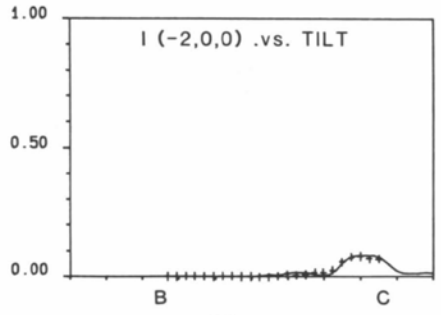

(*b*)

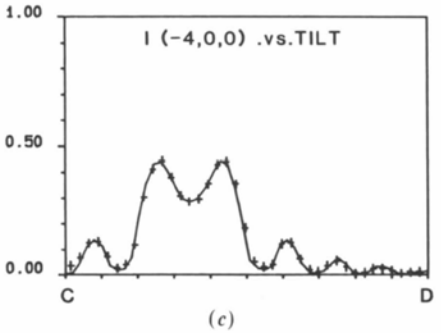

(*c*)

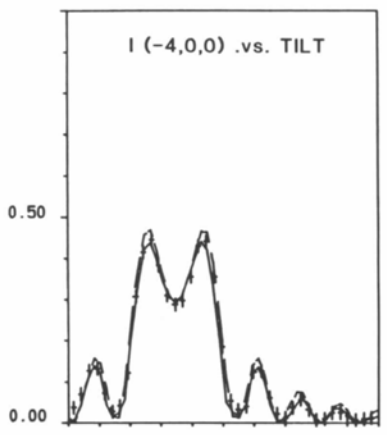

(*d*)

Fig. 7. (*a*), (*b*) and (*c*) Comparison of theoretical (continuous line) and experimental (crosses) rocking curves for the 000, 200 and 400 CBED disks respectively in GaAs at 120 kV. (*d*) The best fit of an effective potential to experimental data (crosses) and the full dynamical calculation (continuous line).

Table 3. *Structure factors in* GaAs *determined by electron diffraction, comparison with theoretical values and results from X-ray diffraction*

Method	Temperature (K)	$g=200$			$g=400$		
		e_{V_g}	x_{F_g}	x_{F_g}†	e_{V_g}	x_{F_g}	x_{F_g}†
Single-crystal X-ray (Matsushita & Hayashi, 1977)	room temp.					141·9 (4)	165·2‡
Powder X-ray (Uno, Okano & Yukino, 1970)	293		−5·2			138·7 (1)	
Convergent-beam electron diffraction (this work)	90	0·432 (9)	5·76	5·80	4·53 (4)	159·0 (10)	163·8
Doyle & Turner (1968) (theory)		0·489*	5·47*	5·56	4·55*	158·6*	163·4
Nielsen & Martin (1985) (theory)				5·92			160·4

* At 90 K using Debye-Waller factor for X-ray conversion from Reid (1983).
† Debye-Waller factor excluded, using data from Reid (1983), average value assumed for Ga and As for experimental data.
‡ Corrected for dispersion, see Nielsen & Martin (1985). No Debye-Waller factor.

the inner subsidiary maxima were used. All other structure factors were taken from the Doyle & Turner (1968) X-ray scattering factors for neutral atoms, with the usual expression for the electron scattering factor:

$$f_{el}(s) = (me^2/2h^2)(Z - f_x)s^2$$

where $s = (\sin\theta)/\lambda$ and the equation is written in CGS units. Debye-Waller factors at 90 K were taken from Reid (1983).

A Bloch-wave eigenvalue calculation based on (3) using a complex non-Hermitian structure matrix representing non-centrosymmetrical GaAs structure with absorption included was first tried and found to agree very closely with the usual perturbation treatment of absorption (Reimer, 1984) which was used in further calculations. The refinement was carried out in several steps. An initial refinement based on ten systematic beams was used to obtain starting values for the adjustable parameter listed above. The result of the final refinement shown in Fig. 7 included all the 45 beams appearing with appreciable intensity in the pattern of Fig. 1 (including HOLZ reflections). The dashed line shows the best fit obtained using the two-beam expressions with $V(400) = 4{\cdot}86$ V. Table 3 summarizes the results and compares them with theoretical and experimental X-ray structure factors for GaAs. The experimental values thus obtained include the Debye-Waller factor. For comparison with theoretical values, a temperature factor has to be assumed (see Nielsen & Martin, 1985).

A careful analysis of errors has been made, using computational trials, the Bethe potential expression [(6)] and differentiation of (1). The results may be summarized thus: (i) The error of 0·5% in thickness determination of 880 Å results in a similar error in the refined value of V_g. (ii) We find that a 10% error in the assumed high-order structure factors results in a 0·1% error in $V(400)$. (iii) The error of 0·5% in accelerating voltage results in a 0·25% error in $V(400)$. (iv) The error of about 1% in excitation error determination has a negligible effect on the disk intensities provided they are not crossed by HOLZ lines in the region of interest. (v) The main effects of absorption are an overall attenuation of the curves for $g=0$; a 5% error in estimated absorption coefficients produced a negligible effect on the structure factors. (vi) Variations in the Debye-Waller factor assumed for the high-order reflections have only a small effect. (vii) The most important experimental source of error results from the convolution of the experimental data with the detector slit. This leads to an error of about 0·5% in the measured values of V_g. In summary, combining these effects we find that the error in our measurements of $V(400)$ is about 1% while that in $V(200)$ is about 2%.

The experimentally obtained 200 and 400 structure factors may be used to determine the distribution of potential or charge in the crystal. In particular, the deviation from the electron distribution corresponding to free atoms can be studied and compared with theoretical calculations of band structure. From Table 3 the experimental 200 structure factor is seen to differ significantly from the theoretical value assuming neutral atoms. On the other hand the deviation of the 400 result from the free-atom value is quite small.

5. Discussion and concluding remarks

The intensity variations within CBED disks offer several possibilities for determination of structure factors. Many features, *e.g.* intensity profiles across CBED fringes, Kikuchi or Kossel lines, can be measured with high accuracy - and often described to a fair approximation by two dominating Bloch waves. We have applied this description to systematic rows in simple structures. The [*h*00] and [*hhh*] rows in GaAs are shown as examples. Theoretical calculations as well as the treatment of experimental intensity curves in the [*h*00] row show that the two-Bloch-wave description with an effective potential is useful and can be accurate to a few percent. The intensity in the strong reflections can be approximated by a two-beam expression for a wide range of orientations around their Bragg condition. For the weaker superstructure

reflections (200 *etc.*) the two-Bloch-wave description may be valid only in a narrow region near the Bragg condition. However, since their intensity is also confined to this region, the two-beam-like expressions can be applied to the weak reflections as well. Exact calculations may thus be reserved for the refinement of structure factors.

The [*hhh*] row shows much less pronounced two-Bloch-wave behaviour for the inner reflections, where strong coupling between neighbouring reflections leads to three-beam-like conditions. However, as we go further out along the [*hhh*] row where the Ewald sphere is steeper, we again find two-beam-like character.

The Bethe potential is found to be a good approximation to U^{eff} (or the gap at the dispersion surface), especially when the other beams are weak in the sense that $U_h/2ks_h$ is small. An iteration procedure for determination of the structure factors from the observed gaps has been developed (Appendix) and applied to theoretical and experimental rocking curves for reflections in a systematic row. In principle this procedure can be applied to an unknown structure.

The various approximations can be evaluated from our experimental results. The direct application of the two-beam form gives the experimentally determined $V(400)^{\text{eff}} = 4{\cdot}86$ V. When introduced in the Bethe series for the systematics case, this gives $V'(400) = 4{\cdot}74$ V - which agrees remarkably well with the result of a many-beam systematic calculation, *viz.* $V(400) = 4{\cdot}75$ V. Our full three-dimensional refinement including all 45 beams indicated in Fig. 1(*b*) gives $V(200) = 0{\cdot}432\,(9)$ and $V(400) = 4{\cdot}53\,(4)$ V. When the electron diffraction determination of structure factors is converted into X-ray values, the relative accuracy is improved considerably for the inner reflections: the error limits of 2 and 1% for $V(200)$ and $V(400)$ respectively correspond to 0·7 and 0·5% in the X-ray scattering factors.

The inner reflections are of particular interest in connection with theoretical calculations of electronic structure. In recent years pseudopotential methods have been applied to calculations of ground-state properties of crystals. By adding a core contribution, this method gives values of X-ray structure factors from first-principle calculations containing no adjustable parameters other than atomic number and crystal structure (*e.g.* Yin & Cohen, 1982). The results of such calculations can therefore be tested by comparison with our experimental values. The structure factors calculated by Nielsen & Martin (1985) are in fair agreement with the values reported here. As seen from Table 3, the electron transfer to As, as given by U_{200}, is slightly less than their calculations. Our experimental 400 value is close to the neutral-atom value, indicating much smaller bonding charge than obtained from the band structure calculations of Nielsen & Martin (1985). A more extensive study of the electron distribution based on measurements of further structure factors is in progress.

In previous measurements of structure factors from CBED fringes (*e.g.* Goodman & Lehmpfuhl, 1967; Voss, Lehmpfuhl & Smith, 1980) photographic methods have been used. The present method, based upon detection through an energy loss spectrometer, has several advantages. The elimination of background and the larger linear range available may be especially important for the weak reflections, where essentially an integrated intensity is measured, normalized to the strong reflection profile. The accuracy may be somewhat poorer than the best critical voltage measurement, but the present method has wider application and does not depend upon knowledge of other structure factors to the same extent.

In the present study we have been concerned with refinement of a few structure factors for a known structure. In principle the calculation methods based upon Bethe potentials - or other approximations to U^{eff} - can be applied also to a row of reflections in an unknown structure, provided a two-Bloch-wave description is adequate as a first approximation. Even in cases where this does not hold for the inner reflection, it may be possible to apply such a procedure to higher orders of the systematic row, since the two-Bloch-wave character becomes more pronounced and reflections better separated with increasing order. This is borne out by the calculations referred to in § 3; note also the interpretation of high-order systematics in purely kinematical terms reported by Taftø & Metzger (1985).

In our study non-systematic reflections were introduced only as a correction, amounting to a few percent. No attempt was made to apply the procedures outlined in § 2 *ab initio* to reflections in a projection. However, such an extension appears feasible, provided measurements can be made of intensity profiles associated with gaps at the dispersion surface. To the extent that experimental values of U^{eff} can be extracted from such measurements, they can be treated by approximate expressions based either upon Bethe potentials or by the perturbation formulae given in § 2 for scattering between rows in a zone. The latter procedure may be compared with the use of HOLZ reflections shown by Vincent, Bird & Steeds (1984).

The representation of intensity features in terms of two-beam-like rocking curves with the 'gap' U^{eff} as parameter appears to be a powerful way of treating CBED data. It should be mentioned that this involves a kind of high thickness approximation in terms of the strong beams present. When the gap is strongly influenced by multiple beam interactions the thickness must be large enough for these to develop. A treatment of this case as given by Gjønnes (1962) may be incorporated in the procedure - or left to the final many-beam refinement.

Part of this work was supported by NSF grant DMR8742108 and by the facilities of the NSF national centre for electron microscopy at Arizona State University (ASU). One of us (JG) is indebted to the Physics Department at ASU for a visiting professorship. We are grateful to Dr M. O'Keefe for many useful discussions.

APPENDIX

Calculation procedure for obtaining Fourier potentials from intensity profiles in a systematic row

The procedure is based upon fitting experimental profiles to the two-beam-type expression

$$I_g(s_g, z) = I_0 \frac{(U_g^{\text{eff}})^2}{(U_g^{\text{eff}})^2 + (ks_g)^2} \sin^2 \{[V_g^2 + (ks_g)^2]^{1/2} z/k\} \qquad (A1)$$

where the symbols have their usual meaning (see § 2) with U_g^{eff} as an effective structure factor. The thickness, effective structure factors and finally the structure factors are to be determined from profiles of different thicknesses in terms of extinction length (see Fig. 8). As an example we give details of the model calculation referred to in § 3, *i.e.* the retrieval of 400, 800 and 200 structure factors from calculated rocking curves.

The thickness was determined from the 400 rocking curve by fitting the maxima and minima of I_{400} which

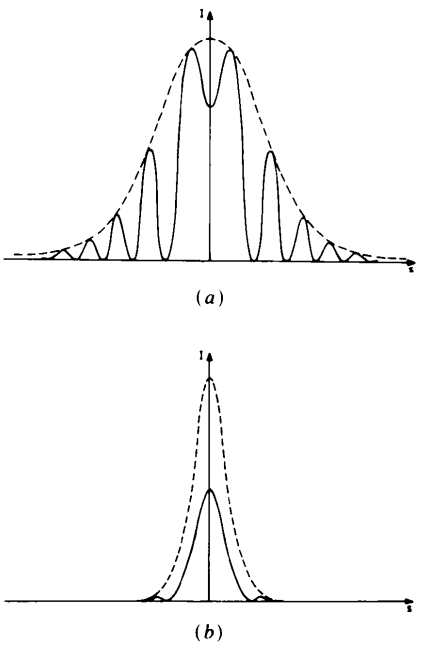

Fig. 8. Typical Kossel line profiles for (*a*) large and (*b*) small gap at the dispersion surface.

are given by

$$[(ks_g)^2 + (U_g^{\text{eff}})^2] z^2 = [(n/2)/\pi]^2. \qquad (A2)$$

If the zeros and maximas are numbered $n_0 + i$ starting with the first zero and s_i are the corresponding excitation errors, the thickness and the gap can be found by a least-squares fit of the positions of the zeros and maxima to

$$[(ks_g)^2 + (U_g^{\text{eff}})^2] z^2 = [(n_0 + i)\pi/2]^2. \qquad (A3)$$

The calculations are performed in two steps: first the values of s_g at minima and maxima of I_g are obtained by fitting the I_g values around these to parabolic expressions. Then we perform a least-squares fit to (*A*3), from which we obtain the thickness z and a preliminary value of U_g^{eff}.

Since this procedure strongly emphasizes the outer part of the rocking curve, it produces a very good value for z. Next the effective potential or gap (and also I_0) must be determined from the part of the curve $I_g^{\text{exp}}(s_g)$ that falls between the first two zeros on either side of the Bragg condition. This is done by calculating

$$\sum_i [I_g^{\text{theory}}(s_i) - I_g^{\text{exp}}(s_i)]^2 \qquad (A4)$$

and varying U_g^{eff} within an interval $U_g^{\text{eff}} \pm \Delta U_g^{\text{eff}}$ until the best fit between the experimental data and the theoretical intensity profile is obtained. For each value of U_g^{eff} we use the following values for the thickness and I_0:

$$z = [(U_g^{\text{eff}})^2 + (ks_g')^2]^{-1/2} (n_0 + 1)/2;$$

$$I_0 = \frac{I_g(s_g = 0)}{\sin^2 (U_g^{\text{eff}} z)} \qquad (A5)$$

where s_g' is the first zero of $I_g^{\text{exp}}(s_g)$.

Since 800 is also a strong reflection the same procedure can be used to determine the corresponding gap, $(U_{800})^{\text{eff}}$. However, the very weak 200 reflection has a narrow intensity distribution near the Bragg condition, usually only one fringe. The method used in the case of the 400 and 800 reflections is therefore not well suited for determination of the 200 gap. Instead we use the integrated intensity of the 200 reflection, *i.e.* the integral

$$\int_{-\infty}^{\infty} I_g^{\text{exp}}(s_g)\, \mathrm{d}s_g.$$

In the two-beam case the integrated intensity can be transformed to an integral of the Bessel function of order zero (Blackman, 1939):

$$\int_{-\infty}^{\infty} I_g(s_g)\, \mathrm{d}s_g \propto A_g \int_0^{A_g} J_0(x)\, \mathrm{d}x, \qquad (A6)$$

where $A_g = U_g z$ and the integral on the right can be calculated or found in tables.

The ratio between the integrated intensity of the 200 reflection and the 400 reflection is then given by

$$\frac{\int_{-\infty}^{\infty} I_{200}(s_{200})\mathrm{d}s_{200}}{\int_{-\infty}^{\infty} I_{400}(s_{400})\mathrm{d}s_{400}} = \frac{A_2 \int_0^{A_2} J_0(x)\,\mathrm{d}x}{A_4 \int_0^{A_4} J_0(x)\mathrm{d}x} \qquad (A7)$$

where $A_2 = (U_{200})^{\mathrm{eff}} z$ and $A_4 = (U_{400})^{\mathrm{eff}} z$. The integrals on the left can be determined from experimental intensity profiles, except for a constant which will not alter the ratio between the two. The integral

$$A_4 \int_0^{A_4} J_0(x)\mathrm{d}x$$

can be calculated from the known thickness and the 400 gap.

The 200 gap can now be determined from the computed value of the integral

$$A_2 \int_0^{A_2} J_0(x)\mathrm{d}x.$$

This equation is solved by Newton's method, or some other iterative method, to give $A_2 = (U_{200})^{\mathrm{eff}} z$.

We use the Bethe formula

$$U_g^{\mathrm{Bethe}} = U_g - \sum_{h \neq g} U_h U_{g-h}/2ks_h \qquad (A8)$$

for the effective Fourier potential (§ 2). A reversal of the Bethe formula will give approximate Fourier potentials or structure factors when the gaps are known. This is achieved by solving the following equations for the U_g's:

$$U_g = k(\gamma^i - \gamma^j) + \sum_{h \neq g} U_h U_{g-h}/2ks_h \qquad (A9)$$

where the sum includes reflections both inside the Ewald sphere (*i.e.* between 0 and g) and outside the Ewald sphere. Separating the reflections inside and outside the Ewald sphere and isolating the terms containing U_g, we find

$$\begin{aligned} U_g(1 + U_{2g}/2ks_{2g}) &= k(\gamma^i - \gamma^j) + 2 \sum_{h<g/2} U_h U_{g-h}/2ks_h \\ &\quad + (U_{g/2})^2/2ks_{g/2} + 2 \sum_{h>g, h \neq 2g} U_h U_{g-h}/2ks_h. \end{aligned} \qquad (A10)$$

These equations are then solved by iteration in the following way. First the gaps, $k(\gamma^i - \gamma^j)_{\min}$, are sorted according to their magnitude. We take the largest gap as a first approximation to the corresponding Fourier potential. For the next strongest reflection, we only take into account the dominating terms in the sum over h, *i.e.* the ones that involve the strongest reflection. All the reflections are treated in this way until approximations for all the U_g's are obtained.

Better approximations to the U_g's are now obtained by inserting the approximate values for the U_h's in the equation. This process is repeated until the U_g's converge, all the time using the new approximations to U_h's as soon as they become available. In the examples studied, we found that the procedure converged whenever the reflections in a systematic row are well separated and the signs of the reflections are correct.

References

BETHE, H. (1928). *Ann. Phys. (Leipzig)*, **87**, 55-129.

BLACKMAN, M. (1939). *Proc. R. Soc. London Ser. A*, **173**, 68-82.

BUXTON, B. F. (1976). *Proc. R. Soc. London Ser. A*, **350**, 335-361.

COWLEY, J. M. (1953). *Acta Cryst.* **6**, 516-521.

DOYLE, P. A. & TURNER, P. S. (1968). *Acta Cryst.* A**24**, 390-397.

FITZGERALD, J. D. & JOHNSON, A. W. S. (1984). *Ultramicroscopy*, **12**, 231-236.

FUKUHARA, A. (1966). *J. Phys. Soc. Jpn*, **21**, 2645-2662.

GJØNNES, J. (1962). *Acta Cryst.* **15**, 703-707.

GJØNNES, J. (1966). *Acta Cryst.* **21**, 240-249.

GJØNNES, J. & GJØNNES, K. (1985). *Ultramicroscopy*, **18**, 77.

GOODMAN, P. (1976). *Acta Cryst.* A**32**, 793-798.

GOODMAN, P. & LEHMPFUHL, G. (1967). *Acta Cryst.* **22**, 14-24.

HØIER, R. (1972). *Phys. Status Solidi A*, **11**, 597-610.

HOWIE, A. (1963). *Proc. R. Soc. London Ser. A*, **271**, 268-287.

MACGILLAVRY, C. H. (1940). *Physica (Utrecht)*, **7**, 329-343.

MATSUSHITA, T. & HAYASHI, J. (1977). *Phys. Status Solidi A*, **41**, 139-145.

MOODIE, A. F., HUMPHREYS, C. J., IMESON, D. & SELLAR, J. (1978). *Inst. Phys. Conf. Ser.* No. 41, pp. 129-134.

NIEHRS, H. & WAGNER, E. H. (1955). *Z. Phys.* **143**, 285-299.

NIELSEN, O. H. & MARTIN, R. M. (1985). *Phys. Rev. B*, **32**, 3792-3805.

REID, J. S. (1983). *Acta Cryst.* A**39**, 1-13.

REIMER, L. (1984). *Transmission Electron Microscopy*. Berlin: Springer.

SHISHIDO, T. & TANAKA, N. (1976). *Phys. Status Solidi A*, **38**, 453-461.

SPENCE, J. C. H. & ZUO, J. M. (1988). Submitted to *Ultramicroscopy*.

TAFTØ, J. (1982). Unpublished report. Institute of Physics, Univ. of Oslo, Norway.

TAFTØ, J. & GJØNNES, J. (1985). *Ultramicroscopy*, **17**, 329-334.

TAFTØ, J. & METZGER, T. M. (1985). *J. Appl. Cryst.* **18**, 110-113.

UNO, R., OKANO, T. & YUKINO, K. (1970). *J. Phys. Soc. Jpn*, **28**, 437-442.

VAINSHTEIN, B. K. & PINSKER, X. G. (1950). *Zh. Fiz. Khim.* **24**, 432.

VINCENT, R., BIRD, D. M. & STEEDS, J. W. (1984). *Philos. Mag.* A**50**, 765-786.

VOSS, R., LEHMPFUHL, G. & SMITH, D. J. (1980). *Z. Naturforsch.* **59**, 973-984.

YIN, M. T. & COHEN, M. L. (1982). *Phys. Rev. B*, **25**, 7403.